International Journal of Heat and Fluid Flow 29 (2008) 1494–1503

Contents lists available at ScienceDirect

International Journal of Heat and Fluid Flow

journal homepage: www.elsevier.com/locate/ijhff

Flow of power-law fluids in simplex atomizers

A. Mandal, M.A. Jog *, J. Xue, A.A. Ibrahim

Department of Mechanical Engineering, University of Cincinnati, Cincinnati, OH 45221-0072, USA

ARTICLE INFO

Article history:
Received 18 December 2007
Received in revised form 10 April 2008
Accepted 27 May 2008
Available online 9 July 2008

Keywords:
Atomization
Non-Newtonian
Computational modeling

ABSTRACT

This paper presents a computational analysis of flow of time-independent, purely-viscous, power-law fluids in simplex atomizers using the volume-of-fluid (VOF) method. Flow of shear-thinning ($0.4 < n < 1$), Newtonian ($n = 1$) and shear thickening fluids ($1 < n < 1.2$) has been considered. The effect of power-law index and atomizer geometry on the flow and atomizer performance has been investigated. Three geometry parameters have been considered, viz., the atomizer constant which is the ratio of inlet area to the product of swirl chamber diameter and the exit diameter, the ratio of swirl chamber diameter to exit orifice diameter, and the length-to-diameter ratio of the exit orifice. The dimensionless film thickness at exit, spray cone angle, and the discharge coefficient for different values power-law index as well as those with varying atomizer geometry are reported. The pressure drop across the atomizer has been kept constant in all simulations. A change in the power-law index significantly alters the flow field in the in the swirl chamber of the atomizer. The velocity magnitudes and liquid film thickness at the orifice exit change with the power-law index. With fixed atomizer geometry, the pseudoplastic fluids tend to produce thinner liquid sheet, larger spray cone angle, and have lower discharge coefficient compared to dilatant fluids. Changes in the atomizer geometry have a significant impact on the flow for all values of power-law index. The spray cone angle decreases and the discharge coefficient and the film thickness increase with increasing atomizer constant. With increasing D_s/d_o, the *dimensionless* film thickness at exit increases whereas the *dimensional* film thickness decreases monotonically. The discharge coefficient increases and the spray cone angle decreases with increasing D_s/d_o. The discharge coefficient, the spray cone angle, and the film thickness decrease with increasing l_o/d_o. A significant finding is that the variations of film thickness, spray cone angle, and discharge coefficient with a change in atomizer geometry are similar for different values of fluid power-law index, although the numerical values depend on the power-law index. This has important implications for atomizer design and industrial applications as most atomizers are designed for, and characterized with, Newtonian fluids.

1. Introduction

Liquid atomization, the process of producing a large number of droplets from bulk liquid, is used in a variety of engineering applications including fuel injection in combustion systems, spray dispersion of consumer products, manufacturing of pharmaceutical products, detergent and food drying in process industries, and in agricultural sprays (Lefebvre, 1989). Pressure-swirl atomizers or simplex atomizers are commonly used for liquid atomization due to their simple design, ease of manufacture, and good atomization characteristics. Many applications involve fluids that exhibit non-Newtonian flow behavior, which include, among others, atomization of aqueous polymeric solutions in manufacture of pharmaceutical products, paint sprays, spray drying of food and detergents, and sprays in healthcare products (Hecht, 2005). Inspite of these applications, the vast majority of studies on liquid atomization using a simplex atomizer have been carried out with Newtonian fluids (Lefebvre, 1989; Ibrahim and Jog, 2006a,b). Atomizers are typically designed for, and tested with, Newtonian fluids. As such investigation of non-Newtonian fluid flow through simplex atomizers is crucial to understand how they will perform while atomizing non-Newtonian fluids in a variety of applications.

A monograph by Lefebvre (1989) provides a detailed review of the studies on pressure-swirl atomizers in the context of fuel injection until 1989. More recent work has been reviewed by Ibrahim and Jog (2006b). A commonly used geometry of a simplex atomizer is shown in Fig. 1. The liquid to be atomized enters the tangential inlet ports (as seen in the top view) which results in developing a strong swirling motion of the liquid in the swirl chamber. A convergent section accelerates the flow as it enters the exit orifice. The swirl motion of the liquid pushes it close to the wall and creates a zone of low pressure along the center line which results in back flow of air in the atomizer. The liquid emanates from the orifice as a conical sheet that spreads radially outwards due to centrifugal force. The liquid sheet becomes unstable and undergoes a

* Corresponding author. Tel.: +1 513 556 1675.
E-mail address: Milind.Jog@uc.edu (M.A. Jog).

0142-727X/$ - see front matter © 2008 Elsevier Inc. All rights reserved.
doi:10.1016/j.ijheatfluidflow.2008.05.006

Nomenclature

A_a	air core area at orifice exit
A_o	orifice area
A_p	total inlet slot area
C_d	discharge coefficient, $\dot{m}/(A_o(2\Delta p/\rho)^{0.5})$
D_s	swirl chamber diameter
d_o	orifice diameter
d_p	inlet port diameter
K	atomizer constant, $A_p/(D_s d_o)$
L_s	swirl chamber length
l_o	orifice length
n	power-law index
p	static pressure
Q	volume flow rate
r_o	orifice radius, $d_o/2$
t	film thickness at exit, t^* dimensionless film thickness, $t/(d_o/2)$
U	average total velocity at the end of orifice
u	axial velocity component
$\vec{u}$	velocity vector
$\bar{u}_o$	average axial velocity at the end of orifice
w	tangential velocity component
$\bar{w}_o$	average tangential velocity at the end of orifice
X	ratio of area of air core to exit orifice area = A_a/A_o
Δp	pressure drop across the nozzle
α_1	volume fraction of phase 1
κ	surface curvature
θ	spray cone half angle
ρ	density
τ	viscous stress

Subscripts

a	air
i	inlet
o	end of orifice

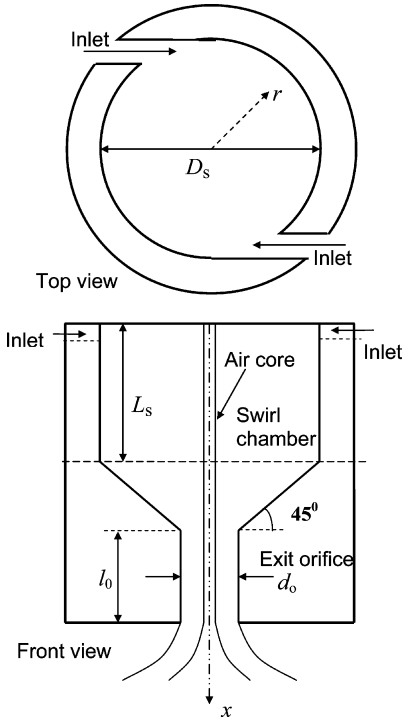

Fig. 1. Sketch of a simplex atomizer.

complex process of breakup to form a spray of droplets. The performance parameters that are of most import are: mean spray droplet size (Sauter mean diameter), droplet size distribution and velocity distribution, the spray cone angle, and the discharge coefficient. The mean drop size roughly correlates with the square root of the film thickness (Lefebvre, 1989). As such the exit film thickness is a significant (but indirect) performance parameter. The mean droplet size, droplet size distribution, velocity distribution and the spray angle impact the speed of subsequent transport processes with the droplets and their mixing with air. Also, the mean droplet size, size distribution and spray angle determine the spread and uniformity of coating in spray coating applications. The discharge coefficient determines the pressure requirement for a desired throughput or determines the possible throughput for a fixed inlet pressure. It is known that the performance of the atomizer is governed by liquid properties, injection flow conditions and the atomizer geometry (Lefebvre, 1989). As the mass flow rate through the atomizer is increased from zero, the performance parameters change sharply at first, but eventually at high mass flow rate, the discharge coefficient, the film thickness, and the spray cone angle become insensitive to the variations in flow Reynolds number. Simplex atomizers are typically designed to operate in this range as a consistent performance can be expected irrespective of small changes in the inlet pressure. As such, in this regime, inlet flow conditions tend to have a small effect on the atomizer performance. Hence most of the work on simplex atomizers has generally focused on investigation of the effect of atomizer geometry and liquid properties on atomizer performance in this flow regime.

Experimental investigations have generally reported measurements of spray angle, pressure drop, and mean drop size with Newtonian liquids, essentially parameters that can be measured outside the atomizer. This is not surprising because in many applications, the atomizer sizes are extremely small (exit diameter of less than 500 μm) which makes direct flow field measurements inside the atomizer extremely difficult. Notable exception for small atomizers is the measurement of film thickness at exit carried out by Suyari and Lefebvre (1986). Lefebvre (1989) and Xue (2004) provide reviews of experimental investigations of the effect of atomizer geometry on the spray angle, discharge coefficient, and mean drop size for Newtonian liquids. Several empirical correlations are available in the literature. However, the predictions of spray angle, film thickness, and drop size tend to differ considerably from each other. Simplified analytical treatment of the flow has been carried out by Giffen and Muraszew (1953); Rizk and Lefebvre (1985, 1986) and Xue et al. (2004), among others. Their results predict the qualitative trends in the effect of atomizer geometry parameters reasonably well. However, the accurate quantitative determination of atomizer performance parameters is not possible with the approximate analyses which in many cases are based on the inviscid flow assumption.

Compared to the large number of publications on the experimental/analytical investigations of Newtonian fluid sprays from simplex atomizers, very few studies are available in the literature which consider flow of non-Newtonian fluids through simplex atomizers (Som, 1983; Som and Biswas, 1986; Schutz et al., 2004) and all of these are restricted to shear-thinning fluids. Som

and co-workers have determined experimentally as well as through an approximate analysis the discharge coefficient and spray cone angle for flow of time-independent, purely viscous, power-law non-Newtonian fluid through a simplex atomizer with purely tangential entry. Theoretical predictions were made through an approximate analytical solution of the hydrodynamics of flow inside the nozzle and experiments were carried out with aqueous solutions of carboxymethyl cellulose sodium salt (CMC) powder of various concentrations as the working fluid. Their experiments were restricted to shear-thinning fluids with the power-law index in the range of $0.7 < n < 1$. Their results confirm that with increasing generalized Reynolds number the values of discharge coefficient and spray cone angle change sharply at first and then become insensitive to the variation in Reynolds number. Their experimental data indicates that at fixed values of generalized Reynolds number based on tangential velocity at the inlet, a decrease in the power index n increases the spray cone angle. The changes in the discharge coefficient were fairly small in the range of power-law index considered by them. Semi-empirical correlations based on their experimental data were provided for discharge coefficient and spray cone angle. Som and Biswas (1986) modified these correlations based on their measurements for flow in simplex nozzles where fluid enters with both the axial and the tangential velocity components. We note that the atomizer geometry considered by Som (1983) and Som and Biswas (1986) differs with the configuration considered here in one significant way. Our geometry includes an exit orifice section (shown in Fig. 1 with length l_o) whereas the geometry used by Som and co-workers does not. It has been shown that the flow velocities and film thickness change considerably as the flow enters the exit orifice section from the nozzle contraction (see for example, Jeng et al., 1998). At the end of the contraction, the fluid has significant radial velocity which produces thick liquid film which becomes thinner as the flow moves in the exit orifice section. The spray cone angle is a function of the ratio of the average swirl velocity to the average axial velocity and is likely to change considerably between end of the contraction and end of the exit orifice. As such the correlations provided by Som and co-workers are not applicable to predict atomizer performance for the atomizers considered here.

To computationally model the flow in a simplex atomizer, one must be able to track the liquid/gas interface accurately. The location of the interface is not known a-priori and must be determined as part of the solution. Furthermore, regions of recirculating flow in the swirl chamber and free surface prediction of the sheet emanating from the atomizer add further complexities in computational modeling of the flow. In recent years, advance computational techniques have been effectively employed to overcome these difficulties. Two methods have been used to accurately track the interface and determine the two-phase flow. First is the Arbitrary-Lagrangian–Eulerian (ALE) method used by our group (Jeng et al., 1998; Sakman et al., 2000; Liao et al., 1999; Xue et al., 2004) and the second is the volume-of-fluid (VOF) method used by Hansen et al. (2002); Dash et al. (2001), and more recently by Ibrahim and Jog (2006a). The ALE method (Hirt et al., 1974) is divided in two steps. The first step is the Lagrangian step where the grid points move with the local velocity. The points on the interface always remain on the interface tracking a sharp interface. The second step is the Eulerian step where a new grid is created by moving points back in the axial direction, and redistributing grid points on the interface. A computational code based on the ALE method to determine the flow in a simplex atomizer was developed by Jeng and co-workers (Jeng et al., 1998; Sakman et al., 2000; Liao et al., 1999; Xue et al., 2004). To validate the code, experiments were conducted on a large scale prototype atomizer made with optical quality plexiglass so that detailed velocity, film thickness, and spray angle measurements could be made (Jeng et al., 1998; Benjamin et al., 1997, 1998; Ma, 2001). Particle-image-velocimetry (PIV) and laser-doppler-velocimetry (LDV) methods and high speed digital camera were used to measure the velocity field in the swirl chamber, the film thickness variation in the exit orifice, the spray angle, and the intact length of the film before breakup (Benjamin et al., 1997, 1998; Ma, 2001). The validated computational code was then used to simulate flow of *Newtonian* fluids through the atomizer under constant mass flow rate condition (Jeng et al., 1998; Sakman et al., 2000 and Xue et al., 2004).

The volume-of-fluid method of Hirt and Nichols (1981) is easy to implement in a computational code and hence it is available in many commercial flow solvers (Fluent, CFX, StarCD, and other). In this method, governing equations for mass conservation and momentum conservation are solved in the entire domain where the density and viscosity of the fluid are calculated as weighted average of the corresponding properties of the two phases based on the phase volume fraction in each cell. In addition to the mass and momentum conservation equations, an equation for the volume fraction of each phase is solved. When the volume fraction is between zero and one, a fluid interface is present within the computational cell. This interface can be recreated by plotting iso-VOF contours by interpolating the volume fraction information at each cell node. The VOF method tends to spread the interface over three cells and typically iso-VOF of 0.5 is used as the location of the interface (Ibrahim, 2006). Dash et al. (2001) and Donjat et al. (2002) used the VOF method to study effect of inlet jets and the development of the swirling flow and air core in the simplex atomizer. They found that the flow is essentially axi-symmetric except for the inlet section. This is further validated from experiments conducted with a large-scale pressure swirl atomizer (Donjat et al., 2002; Jeng et al., 1998). Hansen et al. (2002) simulated the flow in a scaled model of a Danfoss pressure-swirl atomizer using commercially available CFX-4.3 code. The simulations were performed in a three dimensional curvilinear grid representing the swirl chamber of the atomizer assuming laminar flow as well as with different methods for turbulence modeling. They showed that simulations assuming laminar flow with VOF method provided the best agreement with measurements of Hansen and Madsen (2001).

2. Mathematical formulation

We consider an incompressible, isothermal, laminar two-phase flow through a pressure-swirl atomizer as shown in Fig. 1. Based on the evidence from experimental measurements conducted on large-scale prototype atomizers (Ma, 2001; Donjat et al., 2002; Jeng et al., 1998), the flow is considered axi-symmetric. Ma (2001) carried out detailed measurements of the flow field in the swirl chamber of a large scale simplex atomizer using particle-image-velocimetry (PIV) and laser doppler velocimetry (LDV) techniques and showed that the flow field in the swirl chamber is axisymmetric even for an atomizer with only two inlet slots. The mass and momentum conservation equations are applied to the entire flow field where the viscosity and density for each cell are evaluated as volume-fraction-weighted-average of the corresponding properties of the individual phases. An equation for the phase volume fraction is solved simultaneously with the mass and momentum conservation equations on a fixed Eulerian structured grid and the volume fraction of each of the phases in each computational cell is tracked throughout the domain. For flow with two-phases, the volume fraction of the cell is denoted as $\alpha_1 = 1$ for a cell containing only the first phase; $\alpha_1 = 0$ for a cell with only the second phase, and $0 < \alpha_1 < 1$when a cell contains the interface between the first and second phase. An equation for the volume fraction $\frac{\partial \alpha_1}{\partial t} + \vec{u} \cdot \nabla \alpha_1 = 0$ is solved simultaneously with the conservation equations governing the flow:

$$\nabla \cdot \vec{u} = 0 \tag{1}$$

$$\rho \frac{D\vec{u}}{Dt} = -\nabla P + \nabla \cdot \vec{\tau} + \rho \vec{f} \tag{2}$$

The generalized Newtonian fluid model is (Bird et al., 2002):

$$\tau = -\eta(\nabla \vec{u} + (\nabla \vec{u})^{t}) = -\eta \dot{\gamma} \tag{3}$$

Here, superscript "t" indicates transpose. According to two-parameter power-law model:

$$\eta = m\dot{\gamma}^{n-1} \tag{4}$$

where n is power index (fluid behavior index) and m is fluid consistency.

The power-law index $n < 1$ indicates shear-thinning or pseudoplastic fluid; whereas $n = 1$ is Newtonian fluid; and $n > 1$ corresponds to shear-thickening or dilatant fluid.

Commercially available CFD solver Fluent 6.3 (2006) was used to solve the governing equations with the geometric reconstruction scheme. The discretization scheme used for pressure was Pressure Staggering Option (PRESTO). The SIMPLE method (Patankar, 1980) for the pressure–velocity coupling and second order upwind schemes were used for the momentum equations. The VOF solution is based on flux reconstruction and satisfies mass conservation. When a cell is near the interface between two phases, the geometric reconstruction scheme is used which represents the interface between fluids using a piecewise linear interface calculation (PLIC) method. In the PLIC method, the interface is approximated by a straight line of appropriate inclination in each cell having a volume fraction greater than zero and less than one. The first step in this reconstruction scheme is calculating the position of the linear interface relative to the center of each partially-filled cell, based on information about the volume fraction and its derivatives in the cell. The second step is calculating the advecting amount of fluid through each face using the computed linear interface representation and information about the normal and tangential velocity distribution on the face. The third step is calculating the volume fraction in each cell using the balance of fluxes calculated during the previous step. The continuum surface force formulation proposed by Brackbill et al. (1992) is used for the grid cells with $0 < \text{VOF} < 1$ for the surface tension force. The continuum surface tension model results in a source term in the momentum equation for cells that contain the interface and it is expressed as a volume force. The surface tension force (F_s) between the primary fluid and the secondary fluid is given by

$$F_s = \sigma\kappa \frac{\rho \nabla \alpha_1}{\frac{1}{2}(\rho_1 + \rho_2)} \tag{5}$$

The curvature, κ, is defined in terms of the divergence of the unit vector, $\vec{n}$:

$$\kappa = \nabla \cdot \underset{\sim}{\vec{n}} = \nabla \cdot \frac{\hat{n}}{|\hat{n}|} \tag{6}$$

where, $\hat{n}$, is the surface normal and is defined as the gradient of α_1.

3. Verification of solution grid independence and model validation

It is essential to establish grid independence of computational results and validate the model with experimental data. To validate the numerical simulation, comparisons with experimental data of Ma (2001) and Benjamin et al. (1998) for discharge parameters, viz., spray cone angle, film thickness, and discharge coefficient for a large-scale prototype atomizer are made. The uncertainty in the measurements in their work was about 5% for discharge coefficient, about 2° in spray angle, and less than 10% in film thickness measurements. The details of the four atomizer geometric configurations considered for validation are listed in Table 1. To ensure grid independence of results, geometry of case 1 was used and results were obtained with successive refinement of grid. With 26,682 and 46,932 cells, the film thickness changed from 2.2579 mm to 2.2704 mm, the discharge coefficient changed from 0.178 to 0.177, and the spray angle remained unchanged at 86.18°. The differences in the results using the two grids are very small and this indicates that 46,932 cell grid is sufficient to get grid-independent results. We note that VOF method does not allow for a sharp jump in density and viscosity at one grid point. To overcome this limitation we have used a non-uniform dense grid such that the grid is finer in the region where the liquid–air interface is expected. The interface is always located in the orifice and extends in the swirl chamber in a cylindrical region around the axis of radius equal to orifice radius. In the orifice section, we have 115 grid points in the radial direction. In our formulation, we determine the film thickness by considering the liquid–air interface at VOF = 0.5. We checked the sensitivity of the liquid film thickness calculation by changing this value by ±20% and found that film thickness evaluated by considering VOF of 0.4 or 0.6 differs from results for VOF = 0.5 by less than 2%.

To compare the computational results with experimental measurements, the assumption of axi-symmetry requires determination of an equivalent "annular" inlet slot instead of the finite number of slots present in the real atomizer. The width of the "annular" slot as well as the radial and tangential velocities at the inlet are calculated by equating the angular momentum, total mass flow rate, and the kinetic energy of the liquid at the inlet ports with those in the experiments. The boundary condition for the inlet was taken to be radial and tangential velocity components. The inlet tangential and radial velocities at the wall of the swirl chamber are obtained as $W_{\text{inlet}} = \frac{Q}{A_p}\frac{(D_s - d_p)}{D_s}$ and $V_{\text{inlet}} = \sqrt{(Q/A_p)^2 - W_{\text{inlet}}^2}$, thus the inlet width can be calculated. The geometric and flow parameters for the cases considered are shown in Table 1. A comparison of numerical predictions and experimental data of Benjamin et al. (1998) for film thickness, spray angle, and discharge coefficient is shown in Table 2. It is seen that the computational results agree well with available experimental data. To further validate the internal flow field predictions, velocity measurements carried out by Ma (2001) using the PIV method

Table 1
Cases of study

	Case 1	Case 2	Case 3	Case 4
Inlet area (mm^2)	203	406	203	203
Exit orifice diameter (mm)	21.6	28.8	28.8	21.6
Exit orifice length (mm)	36.7	40.5	40.5	36.7
Swirl chamber diameter (mm)	76	76	76	76
Swirl chamber length (mm)	38	38	38	89
Mass flow rate (kg/s)	0.5	0.95	0.95	0.63

Table 2
Comparison of computational results with experiments of Benjamin et al. (1998)

	Case 1	Case 2	Case 3	Case 4
	Film thickness (mm)			
CFD	2.27	3.02	2.18	2.47
Experiment	2.24	3.06	2.41	2.37
	Spray cone half angle (°)			
CFD	43.09	37.88	45.30	41.19
Experiment	42.4	38.5	45.0	38.5
	Discharge coefficient			
CFD	0.177	0.218	0.133	0.150
Experiment	0.17	0.20	0.12	0.16

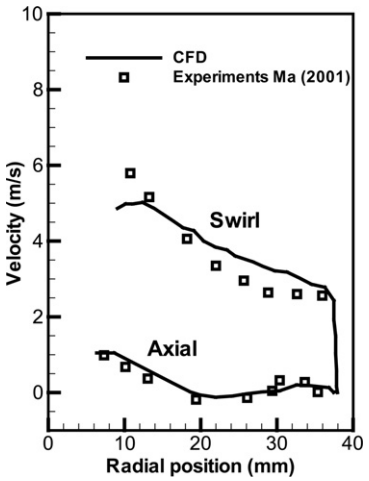

Fig. 2. Comparison of computed axial and swirl velocity profile in the swirl chamber with experimental measurements of Ma, 2001.

are compared with our numerical predictions in Fig. 2. The variation of tangential velocity along the radial direction is shown and the axial velocity variation is shown in Fig. 2 at one location in the swirl chamber of a large-scale prototype of Ma (2001) for liquid phase only. The agreement between numerical solution and experimental data is excellent except for swirl velocity near the liquid/gas interface. Also, our predictions of swirl velocity component are slightly higher than Ma's measurements. As described by Ma (2001), the PIV method requires seeding particles to be introduced in the flow. Although particle density is close to that of liquid, very few particles flow close to the interface due to the high centrifugal force caused by the swirling motion. As a result the uncertainty in the measurements close to the liquid/gas interface is high. Our predictions of swirl velocity components are slightly higher than measurements of Ma (2001) which is not surprising. For one case, Ma (2001) compared his particle-image-velocimetry (PIV) measurements with laser-doppler-velocimetry (LDV) measurements and found that the agreement was within 15% with LDV measurements being generally higher than those obtained by PIV. For a swirl dominated flow, the reason for this difference in swirl velocity component is explained in Ma (2001) as "*Even though a fluid particle experiences a curved trajectory from one point to another during a fixed time interval, PIV processing uses a straight line between the two points to derive the velocity vector. This will underestimate the tangential velocity as the time interval increases.*" It is likely that our predictions of swirl velocity component are higher than PIV measurements due to under prediction of swirl velocity component in the PIV method as described by Ma (2001) and the numerical results are within experimental uncertainty throughout the domain. It is interesting to note that Ma (2001) found that the agreement between the axial velocity measurements by the two methods (PIV and LDV) was excellent. Our axial velocity predictions match with his PIV measurements very well.

4. Results and discussion

The shear-thinning and shear-thickening fluid rheology is expected to alter the flow field in the atomizer and the properties of the liquid sheet emanating from it, and this is investigated using the validated computational model. The effect of power-law index on atomizer performance was investigated keeping the pressure drop across the atomizer constant for shear thinning ($0.4 < n < 1$), Newtonian ($n = 1$), and shear thickening ($1 < n < 1.2$) fluids. Streamline plots for two fluids, $n = 0.6$ and $n = 1.2$ are compared in Fig. 3. The streamlines are based on the axial and the radial component of velocity and do not include the swirl component of velocity which is perpendicular to the plane of the figure. As the flow is assumed to be axi-symmetric, only half of the flow domain is shown. Large recirculatory vortex structures are present in the swirl chamber in both cases, however, their numbers, sizes, and locations are significantly different. As the flow enters the exit orifice section it is pushed along the orifice wall forming a thin liquid

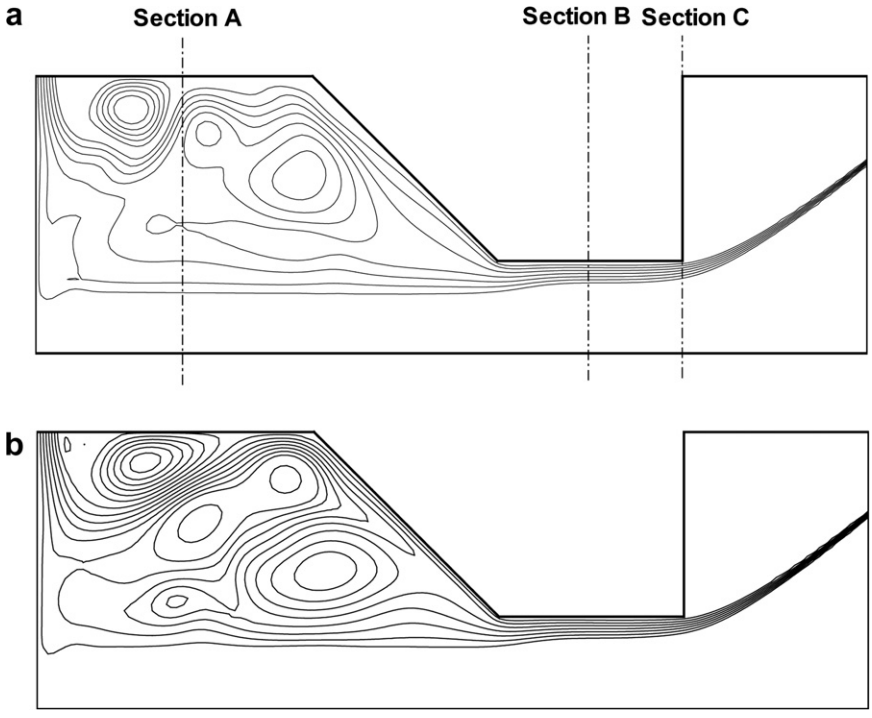

Fig. 3. Streamlines: (a) $n = 0.6$ and (b) $n = 1.2$.

film and the radial component of velocity becomes negligible. The streamlines become nearly parallel to each other indicating liquid moving along the wall with axial and swirl velocity components only. Detailed axial and swirl velocity variation at three axial locations, viz., middle of the swirl chamber, middle of the orifice, and at the exit plate, are shown in Figs. 4a and b. The variations for $n = 0.6$ and $n = 1.2$ are shown by solid and dashed lines, respectively. Once again the most significant differences are seen at section A which is the midpoint of the swirl chamber. In the exit orifice, at section B and C, the velocity variations for the two values on n tend to become similar. In the swirl chamber, both the axial and the swirl velocity components are maximum near the gas–liquid interface. As the flow enters the exit orifice section, fluid accelerates near the wall and the velocity profiles tend to become relatively uniform in the liquid phase at the midpoint of the exit orifice (section B).

Three geometry parameters are known to have the most influence on the flow though the atomizer for Newtonian fluids (Giffen and Muraszew, 1953; Rizk and Lefebvre, 1984, 1985; Lefebvre, 1989; Sakman et al., 2000; Xue, 2004) viz., the atomizer constant or the ratio of inlet area to the product of swirl chamber diameter and the exit orifice diameter ($K = A_p/(D_s d_o)$), the ratio of the swirl chamber diameter to the exit orifice diameter (D_s/d_o), and the ratio of exit orifice length to diameter (l_o/d_o). These parameters are varied and the internal flow and performance of the atomizer in terms of dimensionless thickness, spray angle, and discharge coefficient were examined. The atomizer constant was varied by changing the inlet slot area. The ratio of D_s and d_o was varied by changing both $D_s$and d_o such that their product $D_s \times d_o$ remained constant. This was necessary to make sure that K remains constant while varying D_s/d_o. The length-to-diameter ratio of the exit orifice was changed by changing the length of the orifice. In all the graphs for each performance parameter, the y-axis scale is kept the same so as to make visual comparisons very easy. For example, variations of the dimensionless film thickness are always shown on a scale from 0.15 to 0.45 and half spray cone angle variations are shown on a scale of 20-50° in all figures.

Fig. 5a shows the variations of dimensionless film thickness and Fig. 5b shows the variations of discharge coefficient and spray angle for different values of power-law index n. Pressure drop across the atomizer is held constant in all cases. For a fixed driving force, a dilatant fluid tends to have lower velocities compared to a Newtonian fluid with the same consistency. Consequently, the average swirling velocities and the average axial velocities are lower for shear-thickening fluid flow than corresponding Newtonian cases. Decrease in the swirl velocity in the exit orifice section reduces the centrifugal force responsible to push the fluid close to the wall and increases the liquid film thickness as seen in Fig. 5a for increasing n. For a fixed pressure drop across the atomizer, the discharge coefficient is proportional to the mass flow rate through the atomizer. Two opposing effects play a role in changing the mass flow rate for the shear-thickening fluid relative to a Newtonian fluid.

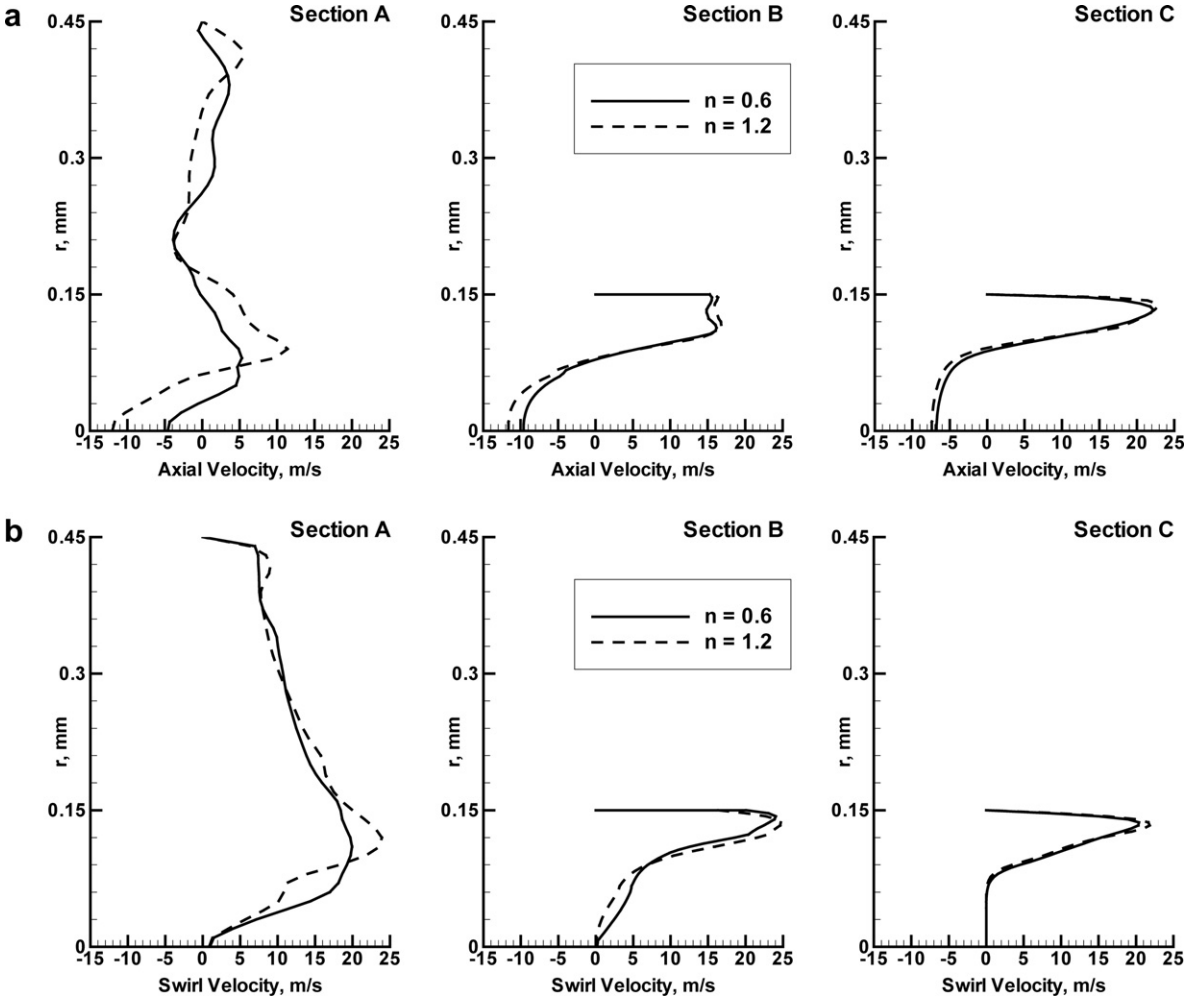

Fig. 4. Velocity variations at three axial locations: (a) axial velocity and (b) swirl velocity.

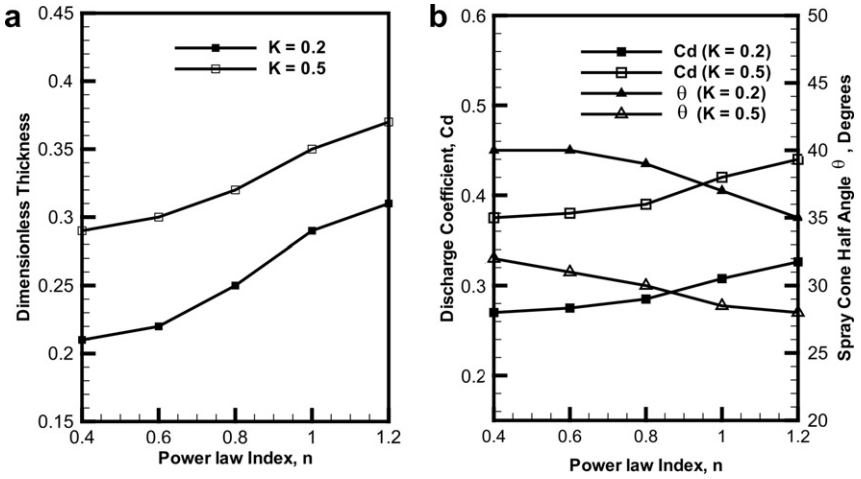

Fig. 5. (a) Variation of dimensionless thickness with power-law index n and (b) variation of C_d and spray cone half angle with power-law index n.

The increase in liquid film thickness which increases the flow cross-sectional area and decrease in velocity have opposite effect on the mass flow rate. The net effect is a slight increase in the discharge coefficient as shown in Fig. 5b. The spray cone angle is proportional to the ratio of the average swirl velocity to the average axial velocity at the exit. The swirl velocity decreases more than the axial velocity with increasing n and lead to a sharp decrease in the spray cone angle. This behavior is consistent with measurements of Som (1983) and Som and Biswas (1986) of discharge coefficient and spray cone angle with variation in power index n. The measurements of Som and co-workers for their atomizer geometry show that both C_d and spray angle have a weak dependence on n for shear-thinning fluids where spray cone angle increased and the discharge coefficient decreased with decreasing n. Similar trends are exhibited in Fig. 5b where the discharge coefficient is seen to decrease slightly and spray cone angle is seen to increase slightly with decreasing n.

The influence of the primary atomizer geometric parameter, the atomizer constant, on the Newtonian and non-Newtonian power-law fluid flow is reported in Figs. 6a and b. Results are presented for three different power-law index values, viz. 0.4, 1.0 and 1.2. The variation of dimensionless film thickness with atomizer constant is shown in Figs. 6a. As atomizer constant K changes from 0.2 to 1, the film thickness increases about 50% in all cases. Increase in K corresponds to increase in inlet area and consequently a decrease in swirl velocity. Therefore, with increasing K, the film thickness increases. It is interesting to see that the effect of atomizer constant is similar for the three values of n shown here although for given atomizer constant value, higher power index produces thicker liquid film. The results are also compared with a correlation Suyari and Lefebvre (1986) for film thickness with a Newtonian fluid flow through the atomizer.

$$0.09\left[\frac{A_p}{D_s d_o}\right]\left[\frac{D_s}{d_o}\right]^{0.5} = \frac{(1-X)^3}{1+X} \tag{7}$$

Here X is the ratio of area of the air core to exit orifice area = A_a/A_o. Suyari and Lefebvre developed their correlation for film thickness by matching their expression for the discharge coefficient to that obtained by Giffen and Muraszew (1953) for inviscid flow. Here X is obtained by solution of the equation derived by Giffen and Muraszew (1953):

$$2(4K/\pi)^2X^2 = (1-X)^3 \tag{8}$$

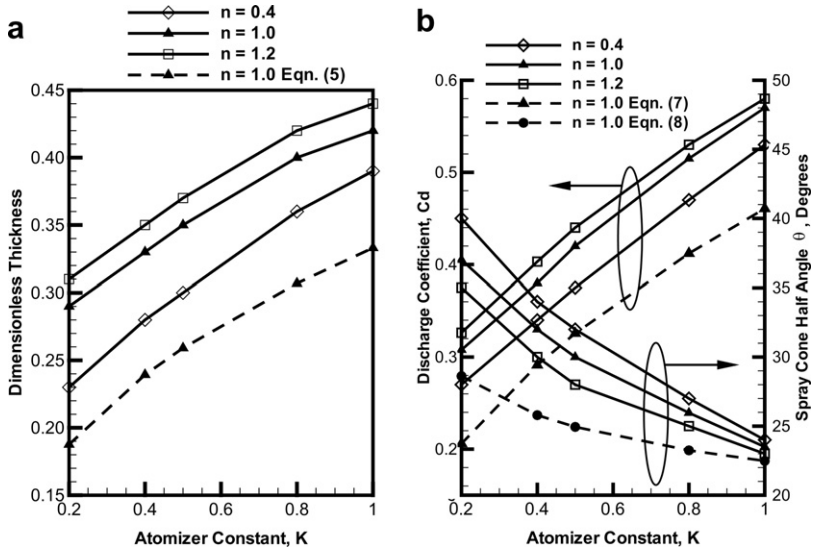

Fig. 6. (a) Variation of dimensionless thickness with the atomizer constant and (b) variation of C_d and spray cone half angle with the atomizer constant.

It is evident that the qualitative behavior shown by these correlations matches our predictions quite well.

Fig. 6b gives variations of discharge coefficient and spray cone angle with atomizer constant. With increasing K, the decrease in swirl velocity results in thicker fluid film. Consequently, the flow cross-section in the exit orifice increases substantially and leads to an increase in the mass flow rate for a fixed pressure drop across the atomizer, and the discharge coefficient increases with increasing atomizer constant. The dashed line shows the variation of discharge coefficient based on a correlation given by Lefebvre (1989):

$$C_d = 0.35\left(\frac{A_p}{D_s d_o}\right)^{0.5}\left(\frac{D_s}{d_o}\right)^{0.25} \tag{9}$$

The values obtained from the above correlation show correct qualitative variation of the discharge coefficient with K but the values are further lower than those for $n = 0.4$. The variation of spray cone half angle with atomizer constant is shown in Fig. 6b. As atomizer constant varies from 0.2 to 1, the spray angle decreases for all values of the power-law index considered. Once again, this is to be expected as lower swirl with higher K would lead to smaller spray cone angle. A correlation given by Rizk and Lefebvre (1985) is used to compare the half spray cone angle results.

$$2\theta = 6K^{-0.15}\left[\frac{\Delta P d_o^2 \rho_L}{\mu_L^2}\right]^{0.11} \tag{10}$$

The results from the correlation are shown by a dashed line which follows the computationally predicted spray cone angle variation. What is noteworthy is that changes in the film thickness, discharge coefficient and the spray angle with varying atomizer constant are similar for shear-thinning, Newtonian, and dilatant fluids, although the numerical values depend on the power-law index.

The variations in dimensionless film thickness, discharge coefficient, and the spray angle are depicted in Figs. 7a and b with varying $D_s/d_o$and show that with increasing D_s/d_o, the discharge coefficient increases, the dimensionless film thickness at the exit increases slightly, and spray cone angle decreases. Note that in this case K was kept constant by keeping $D_s \times d_o$ constant and the ratio of D_s and d_o was varied by changing both D_s and d_o. As such a large value for the diameter ratio is a configuration where liquid is pushed through a small orifice from a large swirl chamber. For a

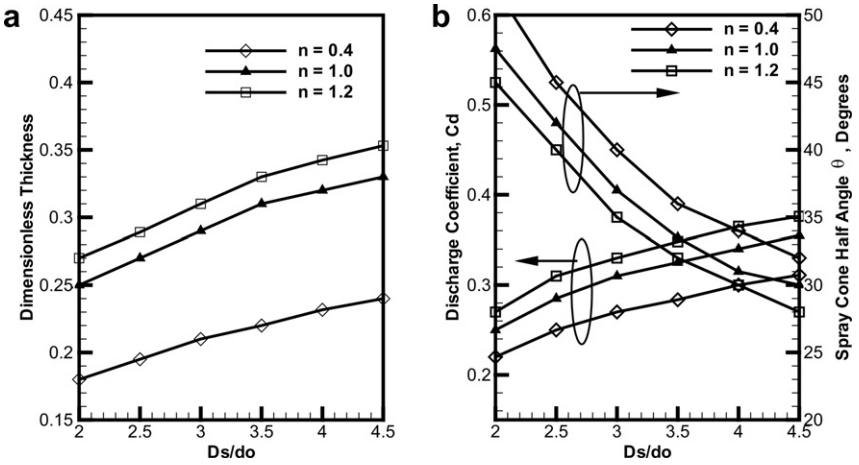

Fig. 7. Effect of D_s/d_o: (a) variation of thickness and (b) variation of discharge coefficient and spray cone half angle.

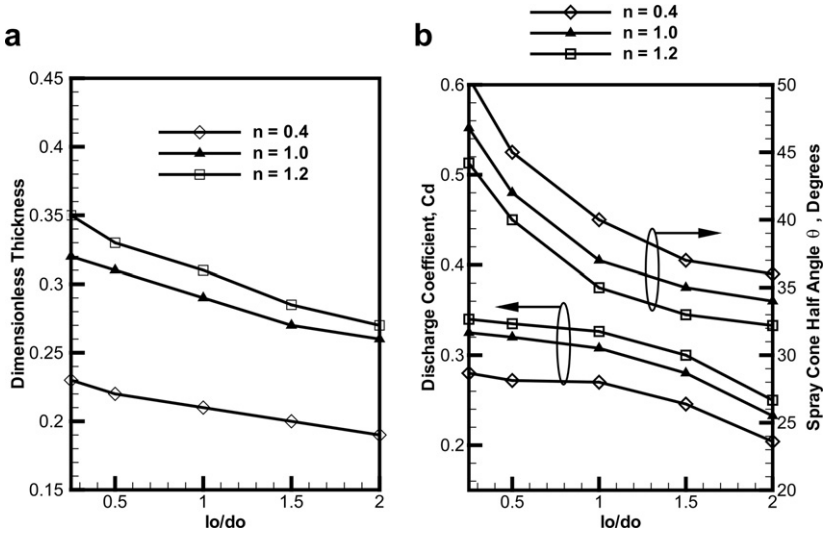

Fig. 8. Effect of l_o/d_o: (a) variation of thickness and (b) variation of discharge coefficient and spray cone half angle.

fixed pressure drop across the atomizer, the axial velocity is expected to decrease when the diameter ratio is high and correspondingly the dimensionless thickness increases slightly. It is found that the absolute film thickness at the exit decreases monotonously with increasing D_s/d_o. Such behavior has been reported in several experimental observations (Lefebvre, 1989). The discharge coefficient increases with increasing D_s/d_o. The increase in the discharge coefficient follows the trend of $\sim(D_s/d_o)^{0.25}$ given by Eq. (7). Also the larger D_s/d_o increases fluid residence time and increases frictional effects on the swirl velocity. Decrease in the swirl velocity with increasing D_s/d_o results in a reduction in the spray cone angle. Once again it is seen that the variations in the performance parameters for the power-law index 0.4 and 1.2 are qualitatively similar to the trends for Newtonian fluid.

Figs. 8a and b show the effect of variation in the exit orifice length-to-diameter ratio. The primary effect of a long exit orifice is to increase the frictional losses in the orifice. As a result the discharge coefficient and the spray cone angle decrease with increasing l_o/d_o. As the flow enters the orifice, the liquid film thickness is large and then decreases sharply along the orifice and then remains nearly constant as seen in Fig. 3. A similar behavior is seen in the variation of dimensionless thickness with l_o/d_o.

5. Conclusions

We have used a computational model based on the volume-of-fluid (VOF) method to investigate the effect of non-Newtonian power-law fluid rheology on the performance of simplex atomizers. Laminar flow of time-independent, purely viscous, power-law fluids (shear-thinning ($0.4 < n < 1$), Newtonian ($n = 1$) and shear-thickening fluids ($1 < n < 1.2$)) was considered. The effect of atomizer geometry was examined by varying three geometric parameters that are known to influence the atomizer performance for Newtonian liquids, viz., the atomizer constant, the ratio of swirl chamber to exit orifice diameter and the ratio of length to diameter of the exit orifice. The results for atomizer performance were presented in terms of dimensionless film thickness at the atomizer exit, the discharge coefficient, and the spray cone angle. From this study we can draw the following conclusions:

1. For the range of power-law index considered in this study, the discharge coefficient and the film thickness increases and the spray cone angle decreases with the power-law index n. The changes in the atomizer performance parameters with varying n are significant for shear-thickening fluids. Slightly weaker variations in C_d and θ are predicted for shear-thinning fluid flow through pressure-swirl atomizer.
2. Since the flow and performance parameters vary with n, for a given atomizer geometry, the spray angle, the discharge coefficient and the thickness of the liquid film exiting from the atomizer could be controlled by changing the rheological properties of liquid (for example, by adding polymeric additives).
3. The atomizer constant has significant effect on atomizer performance for all values of power-law index considered. Increase in K gives higher film thickness at exit, larger discharge coefficient and lower spray cone angle. The variations in atomizer performance parameters with K are similar for all the values of n consider here.
4. For the atomizer geometries considered in the study, the dimensionless film thickness increases slightly with increasing D_s/d_o. However, the dimensional film thickness decreases monotonically with decreasing exit orifice diameter.
5. Added frictional effect in a long orifice cause the discharge coefficient and spray angle to decrease with l_o/d_o.
6. What is noteworthy is that changes in the film thickness, discharge coefficient and the spray angle with varying atomizer geometry are similar for shear-thinning, Newtonian, and dilatant fluids, although the numerical values depend on the power-law index. This has important implications for atomizer design and industrial usage as most atomizers are designed for and characterized with Newtonian fluid flow through the atomizer.

Acknowledgement

Support for this work by the University Research Council of the University of Cincinnati is thankfully acknowledged.

References

Benjamin, M.A., Jeng, S.M., Jog, M.A., 1997. Comparison of simplex atomizer correlations with detailed CFD and experimental data. In: Proc. Tenth Annual Conference on Liquid Atomization and Spray Systems, Irvine, CA. Institute for Liquid Atomization and Spray Systems.

Benjamin, M.A., Mansour, A., Samant, U.G., Jha, S., Liao, Y., Harris,T., Jeng, S.M., 1998. Film thickness, droplet size measurements and correlations for large pressure-swirl atomizers. In: Proc. International Gas Turbine and Aeroengine Congress and Exhibition, American Society of Mechanical Engineers, Stockholm, Sweden. 98-GT-537.

Bird, R.B., Stewart, W.E., Lightfoot, E.N., 2002. Transport Phenomena. Wiley, New York.

Brackbill, J.U., Kothe, D.B., Zemach, C., 1992. A continuum method for modeling surface tension. Journal of Computational Physics 100 (2), 335–354.

Dash, S.K., Halder, M.R., Peric, M., Som, S.K., 2001. Formation of air core in nozzles with tangential entry. Journal of Fluids Engineering 123 (4), 829–835.

Donjat, D., Estivalezes, J.L., Michau, M., 2002. In: Proc. of 15th Annual ILASS Conference, Institute for Liquid Atomization and Spray Systems , Madison, WI..

Fluent-Inc., 2006. Fluent 6.3, Lebanon, NH.

Giffen, E., Muraszew, A., 1953. The Atomisation of Liquid Fuels. John Wiley, New York.

Hansen, K.G., Madsen, J., Trinh, C.M., Ibsen, C.H., Solberg, T., Hjertager, B.H., 2002. A computational and experimental study of the internal flow in a scaled pressure-swirl atomizer. In: Proc. ILASS-Europe, Institute of Liquid Atomization and Spray Systems, Zargoza.

Hansen, K.S., Madsen, J., 2001. A Computational and Experimental Study of the Internal Flow in a Scaled Pressure-Swirl Atomizer. Aalborg Universitat, Esbjerg.

Hecht, J.P., 2005. Key challenges in atomization in consumer product manufacturing. In: Proc. 18th Annunal Conference of ILASS, Institute for Liquid Atomization and Spray Systems, Irvine, CA.

Hirt, C.W., Amsden, A.A., Cook, J.L., 1974. An arbitrary Lagrangian–Eulerian computing method for all flow speeds. Journal of Computational Physics 14 (3), 227–253.

Hirt, C.W., Nichols, B.D., 1981. Volume of fluid method for the dynamics of free boundaries. Journal of Computational Physics 39, 221–225.

Ibrahim, A.A., 2006. Comprehensive Study of Internal Flow Field and Linear and Nonlinear Instability of an Annular Liquid Sheet Emanating from an Atomizer. University of Cincinnati, Cincinnati.

Ibrahim, A.A., Jog, M.A., 2006a. 3D Simulation of flow in pressure-swirl atomizers. In: Proc. Nineteenth Annual Conference of ILASS, Institute for Liquid Atomization and Spray Systems, Toronto, Canada.

Ibrahim, A.A., Jog, M.A., 2006b. Dynamics of two-phase flow in pressure-swirl atomizers. Recent Research Developments in Applied Physics 9, 1–20.

Jeng, S.M., Jog, M.A., Benjamin, M.A., 1998. Computational and experimental study of liquid sheet emanating from simplex nozzle. AIAA Journal 36 (2), 201–207.

Lefebvre, A.H., 1989. Atomization and Spray. Hemisphere Publishing, New York.

Liao, Y., Sakman, A.T., Jeng, S.M., Jog, M.A., Benjamin, M.A., 1999. A comprehensive model to predict simplex atomizer performance. Journal of Engineering for Gas Turbine and Power 121, 285–294.

Ma, Z., 2001. Investigation on the Internal Flow Characteristics of Pressure-Swirl Atomizer. University Of Cincinnati, Cincinnati.

Patankar, S.V., 1980. Numerical Heat Transfer and Fluid Flow. Hemisphere Publishing, New York.

Rizk, N.K., Lefebvre, A.H., 1984. Spray Characteristics of Simplex Swirl Atomizers. Progress in Aeronautics and Astronautics 95, 563–580.

Rizk, N.K., Lefebvre, A.H., 1985. Internal flow characteristics of simplex swirl atomizers. Journal of Propulsion and Power 1, 193–199.

Rizk, N.K., Lefebvre, A.H., 1986. Influence of liquid properties on the internal flow characteristics of simplex atomizers. Atomization and Spray Technology 2, 219–233.

Sakman, A.T., Jog, M.A., Jeng, S.M., Benjamin, M.A., 2000. Parametric study of simplex fuel nozzle internal flow and performance. AIAA Journal 38, 1214–1218.

Schutz, S., Breitling, M., Piesche, M., 2004. Atomization of suspensions of shear-thinning behavior by aerodynamic wave breakup. Chemical Engineering Technology 27 (6), 619–624.

Som, S.K., 1983. Theoretical and experimental studies on the coefficient of discharge and spray cone angle of a swirl spray pressure nozzle using a power-law non-Newtonian fluid. Journal of Non-Newtonian Fluid Mechanics 12, 39–68.

Som, S.K., Biswas, G., 1986. Coefficient of discharge and spray cone angle of a pressure nozzle with combined axial and tangential entry of power-law fluids. Applied Scientific Research 43, 3–22.

Suyari, M., Lefebvre, A.H., 1986. Film thickness measurements in simplex swirl atomizer. Journal of Propulsion 2 (6), 528–533.

Xue, J., 2004. Computational Simulation of Flow Inside Pressure-Swirl Atomizers. University of Cincinnati, Cincinnati.

Xue, J., Jog, M.A., Jeng, S.M., Benjamin, M.A., 2004. Effect of atomizer geometry on the performance of simplex atomizer. AIAA Journal 42 (12), 2408–2415.